

Catalysis Science & Technology

Accepted Manuscript



This article can be cited before page numbers have been issued, to do this please use: X. Yang, Y. Min, S. Li, D. Wang, Z. Mei, J. Liang and F. Pan, *Catal. Sci. Technol.*, 2018, DOI: 10.1039/C7CY02614E.



This is an Accepted Manuscript, which has been through the Royal Society of Chemistry peer review process and has been accepted for publication.

Accepted Manuscripts are published online shortly after acceptance, before technical editing, formatting and proof reading. Using this free service, authors can make their results available to the community, in citable form, before we publish the edited article. We will replace this Accepted Manuscript with the edited and formatted Advance Article as soon as it is available.

You can find more information about Accepted Manuscripts in the [author guidelines](#).

Please note that technical editing may introduce minor changes to the text and/or graphics, which may alter content. The journal's standard [Terms & Conditions](#) and the ethical guidelines, outlined in our [author and reviewer resource centre](#), still apply. In no event shall the Royal Society of Chemistry be held responsible for any errors or omissions in this Accepted Manuscript or any consequences arising from the use of any information it contains.



Journal Name

ARTICLE

Conductive Nb-doped TiO₂ Thin Films with the Whole Visible Absorption to Degrade Pollutants[†]

Xiaoyang Yang, Yuxin Min, Sibai Li, Dawei Wang, Zongwei Mei,* Jun Liang and Feng Pan*

Received 00th January 20xx,
Accepted 00th January 20xx

DOI: 10.1039/x0xx00000x

www.rsc.org/

Titanium dioxide (TiO₂) is widely applied as a photocatalyst but limited by its wide band gap. It is challenging and interesting to make TiO₂ absorb the whole spectrum range of visible light. In this work, conductive Nb-doped TiO₂ (NTO) thin films were demonstrated to increase the photocatalytic performance of anatase TiO₂ due to the whole visible-light absorption and efficient charge transfer. Interestingly, the origin of the whole visible absorption was ascribed to the extended free-carrier absorption (FCA) based on the theoretical calculation and electrical properties. The NTO thin film with high degree of (004) orientation showed better photocatalytic performance than others due to the better absorption, the more effective charge transfer and the greater ability to completely degrade pollutants. In addition, a synergistic effect for the enhancement of photocatalytic performance was observed when thin films were irradiated by alternating the LED light source between 365 nm and 515 nm. We also demonstrate that these thin films are suitable for self-cleaning coatings.

1. Introduction

With the development of industrialization, environmental pollution has been one of the major problems. Many researchers have focused on the study of environmental remediation technologies and environment-friendly materials.¹⁻³ Titanium dioxide (TiO₂) has attracted much attention for photocatalytic applications due to its outstanding performance, rich abundance, low cost, high stability, and environment-friendly features.⁴⁻⁸ However, the wide band gap (~3.20 eV) makes it only be sensitive to ultraviolet (UV) light, which accounts for less than 5% of the solar energy.

In order to utilize visible (Vis) light for the photocatalytic application of TiO₂, many efforts have been devoted, such as impurity doping,⁹⁻¹³ constructing heterojunction,^{14,15} and localized surface plasmon resonance (LSPR) by noble metals.^{6,16} Though these approaches are effective to create visible-light-sensitive TiO₂, they suffer from limited enhancement of light absorption or high cost. Hence, it is still a great challenge to make TiO₂ absorb the whole range spectrum of sun light.

Niobium-doping (Nb-doping) is widely used to improve photocatalytic activities of anatase TiO₂ due to its crystal structure, electrical properties and absorption characteristics.¹⁷⁻²⁵ Firstly, Nb-doping will induce structural

evolution from rutile to anatase and improve photocatalytic activity of TiO₂.¹⁹ Secondly, the pentavalent niobium ion (Nb⁵⁺) doping into TiO₂ introduces more electrons in the conduction band. These excess electron could assist the speedy initial reaction of the organic decomposition process.^{22,23} What is more, Nb-doping is reported to narrow the bandgap and make TiO₂ visible-light-sensitive due to the formation of some shallow donor or defect levels below the conduction band edge.^{17,20} However, Nb-doped TiO₂ (Nb:TiO₂, NTO) has not been reported to absorb the whole range spectrum of visible light as well as we know.

Recently, the NTO film with high degree of (004) orientation have been reported to performance conductive properties with decreased visible transmittance in our previous work.²⁶ It is also a potential candidate as an effective photocatalysis.²¹ The thin film could create a beneficial way to improve photocatalytic performance from two aspects. On the one hand, high percentage of exposed (001) facets will enhance photocatalytic activities of TiO₂.^{15,18,27} On the other hand, the decreased visible transmittance provides a novel way to use the whole range spectrum of visible light for photocatalysis. In addition, the good photocatalytic performance could make the thin film interesting and attractive for self-cleaning coating applications.

In this work, we demonstrate that conductive thin films based on anatase NTO can increase photocatalytic activities of anatase TiO₂ due to the extended free-carrier absorption (FCA) of visible-light and efficient charge transfer. The origin of FCA was studied by the theoretical calculation of electronic structure and electrical measurements, and was demonstrated by the UV-Vis absorption spectra of TiO₂ and NTO. In addition, the photocatalytic activities are also effected by the crystal

School of Advanced Materials, Peking University Shenzhen Graduate School, 2199 Lishui Road, Shenzhen 518055, P. R. China. E-mail: meizw@pkusz.edu.cn (Z. Mei); panfeng@pkusz.edu.cn (F. Pan). Tel: 86-755-26033200 (F. Pan).

[†] Electronic Supplementary Information (ESI) available: Simulated calculation of electronic structure, Rietveld refinement, full EDS Data, XPS spectra, AFM height images and additional photocatalytic degradation figures of TiO₂ and NTO Thin Films. See DOI: 10.1039/x0xx00000x

structure of NTO. The NTO thin film with high degree of (004) orientation shows better photocatalytic performance than others due to the better absorption, the more effective charge transfer and the greater ability to completely degrade pollutants. Furthermore, a synergistic effect for photocatalytic performance is observed for the thin film when alternating irradiation under 365 nm and 515 nm LED light was used. The application as self-cleaning coatings is also demonstrated by investigating the wettability for these thin films.

2. Experimental

2.1 General film preparation

TiO₂ and NTO thin films with random orientation (TiO₂-RO, NTO-RO) and high degree of (004) orientation (TiO₂-004, NTO-004) were deposited by adjusting sputtering angles of DC magnetron sputtering. TiO₂ and NTO thin films were sputtered onto 3 × 3 cm² soda-lime glass substrate (GULUO GLASS) using a oxide target (Φ 6 cm). The TiO₂ thin film was prepared from pure TiO₂ target. The NTO thin film was prepared from a TiO₂ target with 5 % atom of Nb dopant (Ti_{0.95}Nb_{0.05}O₂, 99.9%, Hzamtarget). The substrate was secured onto a 6 × 6 cm² piece of stainless steel substrate holder with a high temperature polyamide tape (2 mm wide). The distance was 8 cm between the center of target and substrate. The base pressure prior to each deposition was 8 × 10⁻⁴ Pa. Films were deposited in pure argon (grade 5.0) at a flow rate of 20 sccm (cubic centimeter per minute at STP) and a system pressure of 0.3 Pa. And the substrate temperature during deposition was 40-60 °C measured with a thermocouple during deposition. A DC sputtering power (SKY Technology Development DC power system) of 40-45 W was required to prepare films with thickness of ~350 nm on the soda-lime glass substrate after 1 h of deposition. Before each deposition, the target surface was sputter-cleaned by pure Ar for 10 min, and then pre-sputtered for 5 min under the film deposition conditions. The as-deposited films were annealed and crystallized in Ar/H₂ (95:5, v/v) atmosphere at a flow rate of 30 sccm in a horizontal furnace at 450 °C for 30 min. The temperature was increased at a rate of 10 °C/min. Then the films were naturally cooled down to room temperature.

2.2 Film analysis

The crystal structure of NTO and TiO₂ films was analyzed using a Bruker D8 Advance powder X-ray diffractometer (XRD) equipped with CuK α radiation with a two-dimensional detector. The scan range of 2 θ was from 10 to 120° and the scan step of 2 θ was 0.02°. The scan time was 1s/step and 2s/step for normal analysis and rietveld refinement, respectively.

Electrical properties of films were measured at room temperature on an Ecopia HMS-3000 Hall effect measurement system set up in the Van der Pauw configuration. Measurements were carried out on 1 × 1 cm² squares, and standard ITO sample was tested prior to any NTO thin films measurements.

Photoelectron spectroscopy studies were performed using a Thermo Fisher ESCALAB 250X surface analysis system equipped with a monochromatized Al anode X-ray source (X-ray photoelectron spectroscopy, XPS, $h\nu=1486.6$ eV).

Optical properties were analyzed over the wavelength range of 300-800 nm using a Shimadzu UV-2450 spectrometer with integrating sphere. The standard sample was newly prepared from anhydrous BaSO₄ powder.

The photoluminance (PL) spectra were measured by a PerkinElmer LS 55 Fluorescence spectrometer with a thin film carrier.

The morphology of thin films was measured using a Zeiss SUPRA-55 Scanning Electron Microscope (SEM).

The content of Nb was investigated via an Oxford-Max 20 energy dispersive Spectrometer (EDS).

The surface morphology, roughness and specific area of thin films were measured and analyzed by Bruker MultiMode 8 AFM (Atomic Force Microscopy) using a tapping model with SCM-PIT probes.

Thin films were characterized by Raman spectroscopy with laser excitation energy of 532 nm in a Horiba iHR320 Raman spectrometer with a cooled CCD detector.

Thickness of films was measured using a Bruker DektakXT profilometer with proper measurement range of 6.5 μ m.

The static contact angles (CAs) were measured with a goniometer (250-F1, DongGuan Precise Test Equipment Co., Ltd). Droplets of distilled water, with a volume of 5 μ L, were placed gently onto the surface at room temperature and pressure. The static CAs of thin films were measured three times at different locations such that the measurement variance was $\pm 2^\circ$.

Photographs were taken using a camera in a Hua Wei Mate 8 mobile phone.

2.3 The degree of preferential (004) orientation ($\eta_{(004)}$)

The degree of preferential (004) orientation could be quantified as follows

$$\eta_{(004)} = \sqrt{\frac{(1-MD_{(004)})^3}{1-MD_{(004)}^3}} \times 100\% \quad (1)$$

where MD(004) is the March–Dollase parameter for the (004) direction and could be obtained from the Rietveld refinement.²⁸

2.4 Catalytic activity test

Photocatalytic degradation of Rhodamine B (Rh B) under simulated solar light irradiation.²⁹ Annealed TiO₂ and NTO thin films were cleaned by ultrasonic treatment in detergent, deionized water, acetone, and isopropyl alcohol for 10 min each and subsequently dried under N₂ flow. Rh B ethanol solution of 10000 ppm was prepared for dye degradation experiment. Subsequently, the prepared solution was spin-coated onto NTO thin films surface at 600 rpm for 30 seconds. As-prepared samples were stored in a glass dish covered with Al foil. After being dried naturally, samples were kept on a plate with constant temperature of 25 °C, and evaluated for photocatalytic activity by monitoring the decolorization of Rh B

under a AM 1.5 illumination via ABET sun 3000 solar simulator. The power of the light was calibrated to one sun light intensity by using a NREL-calibrated Si cell (Oriol 91150). After a specified time, the maximum peak of absorbance band was monitored by a UV-Vis spectrophotometer (Shimadzu UV-2450) to estimate the amount of Rh B. According to the Lambert-Beer law, the absorbance is proportional to the concentration of a dilute solution, from which degradation of Rh B could be describe as follow,

$$\ln \frac{C_0}{C} = kt \quad (2)$$

where C_0 is the initial concentration of the Rh B solution, C the concentration at a specified irradiation time, k the reaction rate, and t the reaction time. We suppose this law could be applied to Rh B molecules on the surface of thin films.

Photocatalytic degradation of Rh B under single-wavelength LED irradiation. Rh B ethanol solution of 120 ppm was prepared for dye degradation experiment. Then 2 mL solution was added in a 10 mL glass bottle. The as-prepared thin film was placed into solution and kept about 20 min. About 1 mL solution was transferred into quartz colorimetric utensil when measured. After the maximum peak of absorbance band monitored to estimate the amount of Rh B, the solution was transferred back to the glass bottle. Then the thin film was irradiated under a single-wavelength LED point light source (SZLAMPLIC, $\phi 3$ mm) with 1×1 cm² light spot. The power of the light was measured by using a normal light meter (CEAULIGHT, CEL-NP2000). After a specified time, the maximum peak of absorbance band was monitored by a UV-Vis spectrophotometer to estimate the amount of Rh B.

3. Results and discussion

3.1 The origin of the whole visible absorption

The optical properties of a material is mainly related to its electronic structure.³⁰ The electronic structures of pure TiO₂ and Nb:TiO₂ (5:95, at%) with anatase structure were calculated using the Vienna Ab-initio Simulation Package (VASP) based on generalized gradient approximation with Hubbard U correction (GGA+U) to the density-functional theory (DFT). The Fermi level of the pure TiO₂ is between the conduction and valence band, indicating no free electrons in the undoped TiO₂ (Figs. 1a and b). Therefore, the pure TiO₂ only shows intrinsic UV absorption. After Nb doping, the Fermi level moves into the conduction band (Figs. 1c and d). There are d-orbital electrons of both Ti and Nb in the conduction band (Fig. 1d). In other words, NTO has free electrons and performs good conductivity.

The existence of free electrons in the conduction band of NTO is also confirmed by the electrical properties of NTO thin films. The electrical properties were characterized by the standard four-probe Hall effect measurements. As listed in Table 1, both NTO-RO (random orientation) and NTO-004 (high degree of (004) orientation) show good conductivity with a low resistivity (on the order of 10^{-4} Ω cm), while TiO₂ shows so high resistivity that it could not be measured by Hall effect

Table 1 Electrical properties of NTO thin films

Sample	Sheet resistance [Ω sq ⁻¹]	ρ [Ω cm]	N [cm^{-3}]	μ [$\text{cm}^2 \text{V}^{-1} \text{s}^{-1}$]
NTO-RO	26.5	9.4×10^{-4}	2.21×10^{21}	3.01
NTO-004	18.6	6.6×10^{-4}	2.13×10^{21}	4.44
TiO ₂	*	*	*	*

* The resistivity of TiO₂-RO and TiO₂-004 is so high that it could not be measured by Hall effect measurements or a two-point probe of Agilent Millimeter.

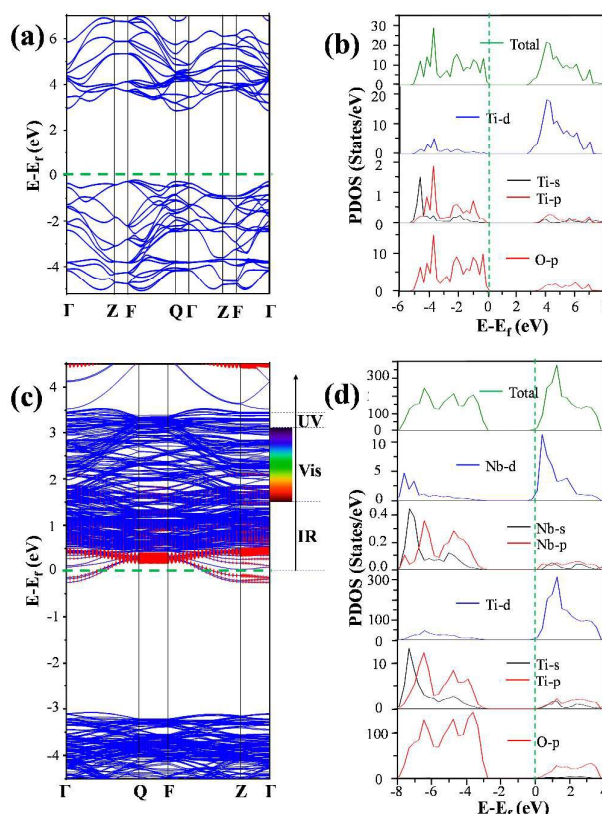


Fig. 1 (a) Electronic band structure of pure TiO₂. (b) PDOS (DOS on specified atoms and orbitals) of pure TiO₂ at the DFT level. (c) Electronic band structure of Nb:TiO₂ (5% of Nb dopant). Blue line represents the band structure of Nb:TiO₂ system. Red dot represents the band structures of Nb. The dot size is proportional to the weight. The green dashed line represents the Fermi level. The spectra card on the right shows a reference of UV-Vis-IR free-carrier absorption. (d) Projected density of states (PDOS) (DOS on specified atoms and orbitals) of Nb:TiO₂ at the DFT level. The Fermi level is at zero energy and marked by the green dashed line.

measurements or a two-point probe of Agilent Millimeter. In addition, the Hall effect measurements indicate that NTO films displayed n-type conductivity, with electrons being the dominant charge carrier species. These results also confirm that the Fermi level of NTO moves into the conduction.

After Nb doping, energy levels of NTO become degeneracy. Degenerate energy levels of NTO make direct FCA available, as conduction-band states are available in the UV-Vis-IR energy range to accommodate the free electrons excited by vertical

transitions (Fig. 1c).^{31–33} Hence, both the intrinsic UV absorption and UV-Vis-IR FCA could occur in NTO. This result is contrast to that of tin dioxide (SnO₂) TCO thin films reported by H. Peelaers,³⁴ but is in good agreement with that of NTO thin films calculated by R. S. Zhang.³⁰

Normally, the FCA is too weak to influence properties of semiconductors, but the FCA becomes significant at high carrier concentrations (on the order of 10²⁰–10²¹ cm⁻³).^{32,34} The carrier concentrations of NTO thin films are on the order of 10²¹ cm⁻³ (Table 1), so the FCA should not be negligible for conductive NTO thin films.

With the theoretical calculation and experiment electrical measurements analysis above, we consider conductive NTO thin films could absorb the whole range spectrum of visible light due to its electronic structure. On one hand, there are abundant free electrons in the conduction band of NTO. On the other hand, energy levels of NTO are degenerate and their conduction-band states are available for the free electrons exciting.

3.2 The preparation, identification and morphology of thin films

To further study the photocatalytic activities and optional properties of NTO, both NTO (5% of Nb dopant) and pure TiO₂ thin films were prepared with random orientation (NTO-RO, TiO₂-RO) and high degree of (004) orientation (NTO-004, TiO₂-004) using our reported method.²⁶

A systematic XRD study shows that both TiO₂ and NTO thin films exhibit typical anatase phase (Fig. 2a). There are no diffraction peaks of rutile or brookite phases. The peaks centred around 25.23° and 37.78° can be ascribed to the (101) and (004) facets of anatase TiO₂. The (101) peaks are stronger than (004) peaks in thin films with random orientation, while the opposite results have been observed in the thin film with

Table 2 Electrical properties of NTO thin films

Sample	MD	$\eta(004)$ (%)	Band gap (eV)	Surface roughness, R _q (nm)	Surface area (μm^2)
TiO ₂ -RO	0.722	18.6	3.34	3.57	1.03
TiO ₂ -004	0.558	32.3	3.29	3.49	1.07
NTO-RO	0.787	13.7	3.43	1.11	1.03
NTO-004	0.482	39.6	3.38	2.57	1.06

high degree of (004) orientation. Compared with the anatase phase of pure TiO₂, the XRD peak position of NTO thin films presents a little shift toward low angle. This is attributed to the doping fact of Nb, because the ionic radius of Nb⁵⁺ (ca. 0.70 Å) is a little larger than that of Ti⁴⁺ (ca. 0.68 Å).

The Le Bail analysis was used to fit the XRD pattern with TOPAS to obtain unit cell parameters, unit volume, and March–Dollase parameter for the (004) direction (Fig. S1 in ESI[†]). The unit cell parameters are $a = 3.786$ Å and $c = 9.504$ Å for the pure TiO₂ thin films (Table S1 in ESI[†]). After Nb doping, both a and c increase around 3.810 Å and 9.540 Å, respectively. The March–Dollase (MD) parameter are fitting to be 0.722, 0.558, 0.787 and 0.482 for thin films TiO₂-RO, TiO₂-004, NTO-RO and NTO-004, respectively. Therefore, the degree of preferential (004) orientation are quantified to be 18.6%, 32.3%, 13.7% and 39.6% for thin films TiO₂-RO, TiO₂-004, NTO-RO and NTO-004, respectively (Table 2). The EDS data of TiO₂ and NTO thin films on soda-lime glass reveal the content of Nb and Ti as listed in Table S2 in ESI[†] (Details are shown in Fig. S2 in ESI[†]). Nb is undetected in pure TiO₂. The doping content of Nb is 8.6 at.% and 8.3 at.% for NTO-RO and NTO-004. The difference of Nb-doping content between the thin film and the target is attributed to that the sputtering yield of Nb atom is a little higher than that of Ti atom.

The typical Raman spectra of TiO₂ and NTO thin films locate between 100 and 700 cm⁻¹ (Fig. 2b). Compared with the pure TiO₂, the E_g mode (around 144 cm⁻¹) of NTO exhibits a blue shift. In addition, as the (004)-oriented growth becomes stronger, E_g mode (around 144 cm⁻¹) of NTO is further blue shift. This result is in good agreement with our previous results.²⁶ The XRD patterns and Raman spectra indicate that anatase thin films are successfully prepared with random orientation and high degree of (004) orientation, respectively.

X-ray photoelectron spectroscopy (XPS) was employed to observe the doping of niobium. No Nb can be detected by XPS measurement in the pure TiO₂. As shown in Fig. 2c, the Ti⁴⁺ peaks with the binding energy (BE) of 458.3 and 464.0 eV are fitted well with XPS spectra for the Ti 2p_{3/2} and Ti 2p_{1/2} transition of pure TiO₂. After Nb doping, the Ti⁴⁺ peaks with the BE of 458.5 and 464.2 eV for the Ti 2p_{3/2} and Ti 2p_{1/2} transition are predominant. However, the reduced titanium state (Ti³⁺) peaks with the BE of 456.8 and 462.8 eV are observed because of the compensating mechanism from redundant electrons of Nb.³⁵ The reduced titanium state makes some asymmetry to the Ti 2p_{3/2} and Ti 2p_{1/2} transition of NTO. Thin films with random orientation and with high degree of (004) orientation

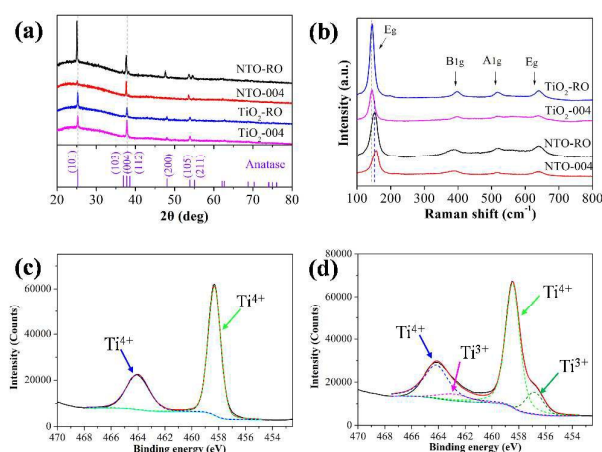


Fig. 2 (a) XRD patterns of anatase TiO₂ and NTO thin films with random orientation (NTO-RO, TiO₂-RO) and high degree of (004) orientation (NTO-004, TiO₂-004). (b) Raman spectra of anatase TiO₂-RO, TiO₂-004, NTO-RO and NTO-004 thin films. (c) XPS spectra of pure TiO₂ thin films showing Ti⁴⁺ state only for the 2p_{3/2} transition. (d) XPS spectra of NTO thin films showing Ti⁴⁺ and Ti³⁺ state for the 2p_{3/2} transition. The data was treated with a Shirley background and individual Gaussian/Lorentzian functions for Ti⁴⁺ and Ti³⁺ final states.

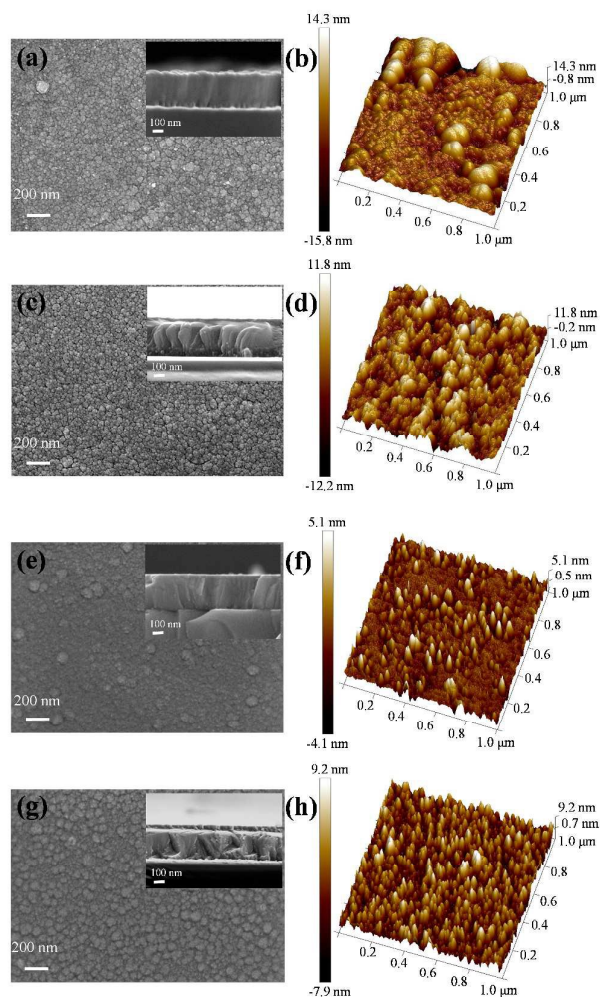


Fig. 3 Top down SEM images and AFM 3D images of thin films TiO₂-RO (a, b), TiO₂-004 (c, d), NTO-RO (e, f) and NTO-004 (g, h). The insets of SEM images depict side on images of thin films.

are show similar results of XPS spectra (Fig. S3 in ESI[†]). These result indicates the formation of Ti³⁺ state and the successful doping of Nb.

Scanning Electron Microscope (SEM) and Atomic Force Microscopy (AFM) images are employed to study the morphology of thin films. As shown in Fig. 3, the surface morphologies are different between pure and Nb-doping TiO₂ thin films. The small particles are spread over the surface of pure TiO₂ thin films (Figs. 3a and c), while some bigger particles could be seen on the surface of NTO thin films (Figs. 3e and g). The side-on images show that the thickness of thin films is ~350 nm. AFM was performed on all positions in 1 μm × 1 μm areas for NTO and TiO₂ thin films (Fig. S4 in ESI[†]). The root-mean-square roughness (R_q) are 3.57, 3.49, 1.11 and 2.57 nm for TiO₂-RO, TiO₂-004, NTO-RO and NTO-004 thin films, respectively. These results indicate that NTO and TiO₂ thin films are compact and smooth (Figs. 3a-h). However, the calculated surface areas are different and measured to be

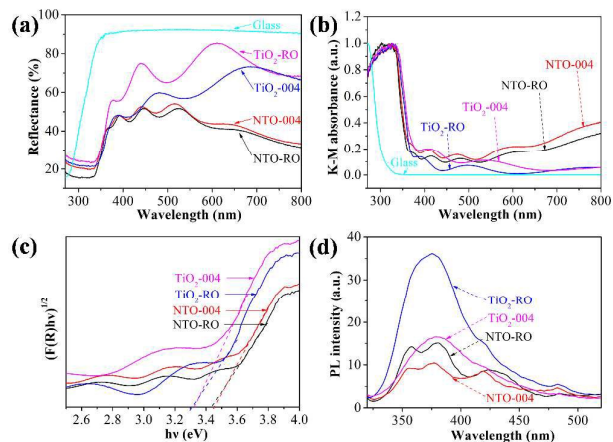


Fig. 4 Diffuse reflectance spectra of TiO₂-RO, TiO₂-004, NTO-RO and NTO-004 thin films and glass substrate. (b) The absorption spectra of thin films and glass substrate converted from DRS by Kubelka-Munk function. (c) Intrinsic optical absorption edges (eV) of thin films. (d) photoluminescence (PL) spectra of thin films for 300 nm laser excitation.

1.03, 1.07, 1.03 and 1.06 μm² for TiO₂-RO, TiO₂-004, NTO-RO and NTO-004 thin films, respectively. AFM 3D images show that particles are cone-shaped on the surface of TiO₂ and NTO thin films (Fig. 3). NTO thin films show more sharply cone-shaped particles than the pure TiO₂. Moreover, the distribution of cone-shaped particles is more dense on the surface of thin films with high degree of (004) orientation than that of thin films with random orientation.

3.3 Electrical and optical properties of thin films

The electrical properties of NTO thin films are listed in Table 1. Both NTO-RO and NTO-004 show good conductivity with carrier concentrations > 2 × 10²¹ cm⁻³. The NTO-004 thin film shows better conductivity than NTO-RO due to the increase of Hall mobility.²⁶ The sheet resistance are as low as 26.5 and 18.6 Ω sq⁻¹ for NTO-RO and NTO-004 thin films. However, the resistivity of TiO₂ thin films is too high to be measured. The electrical properties of NTO and TiO₂ thin films indicate that free electrons are of high concentration in NTO but unobserved in TiO₂. This result makes UV-Vis-IR FCA occur in NTO thin films.

The UV-Vis absorbance spectra of NTO-RO, NTO-004, TiO₂-RO and TiO₂-004 were converted from reflectance to absorbance using the Kubelka-Munk method (Figs. 4a and b). Compared with the pure TiO₂, NTO thin films shows a better absorption property in the region of 550-800 nm, indicating Nb-doping significantly modifies visible light absorption characteristics of TiO₂. This result is in good agreement with our analysis of simulated calculation. Moreover, absorption properties between random orientation and high degree of (004) orientation show a slight difference because of the anisotropy of dielectric function for TiO₂ along different crystal orientation.³⁶ With the analysis above, NTO with both random orientation (NTO-RO) and high degree of (004) orientation

(NTO-004) could absorb the whole range spectrum of visible light.

Fig. 4c depicts intrinsic optical bandgaps of TiO₂ and NTO thin films by constructing Tauc plots using the $(\alpha h\nu)^{1/2}$ relation. The values of Tauc's gap (E_g) are evaluated from the extrapolation of high energy points to intercept on the energy axis with little absorption. The indirect bandgaps are determined to be 3.43, 3.38, 3.34 and 3.29 eV for NTO-RO, NTO-004, TiO₂-RO and TiO₂-004 thin films, respectively. After Nb doping, an obvious blue shift is found for the intrinsic UV absorption edge of conductive NTO thin films. This result can be rationalized by the Burstein-Moss effect, which increases the optical band gap as electrons populate the conduction band.^{26,37} This result is different from the effect of Nb-doping in non-conductive Nb-doped TiO₂ powder. Narrowed bandgaps are observed because of the formation of some shallow donor or defect levels below the conduction band edge.^{17,20} This result also confirms that the Fermi level of NTO moves into the conduction.

Fig. 4d shows the photoluminescence (PL) spectra of TiO₂-RO, TiO₂-004, NTO-RO, and NTO-004 thin films under 300 nm laser excitation. After Nb doping, there are two more emission centers than pure TiO₂, which results from the change of energy bands. The emission peaks around 360 (3.4 eV), 380 (3.3eV) and 430 (2.9 eV) nm are attributed to the radiative recombination of electrons in super-band-gap states, shallow complex $(\text{Nb}_{\text{Ti}}\text{-V}_{\text{Ti}})^{3-}$ states and O_i^{2-} states with holes in the valence band, respectively.¹⁷ The emission peaks around 480 nm (2.55 eV) are attributed to the radiative recombination of electrons in super-band-gap states with holes in surface peroxy states.²⁰ However, the general trend of photoluminescence spectra intensity is TiO₂-RO > TiO₂-004 > NTO-RO > NTO-004. It indicates that Nb doping can decrease the PL intensity. The NTO-004 thin film shows the lowest radiative recombination of photoexcited electron-hole pairs. Three reasons devote to the improvement of charges separation of NTO-004. Firstly, the introduction of Nb⁵⁺ into the TiO₂ structure could improve the conductivity as shown in Table 1. It facilitates the migration of photoexcited electrons to NTO surface and suppresses their recombination. Secondly, the charge mobility becomes higher due to that the static effective mass m^* along α axis ($m_{(100)}^*$) is lesser than that along the c axis ($m_{(001)}^*$).³⁸ Finally, the transfer and separation of photogenerated charges could be enhanced when the percentage of (004) facets increases.¹⁵

3.4 The photocatalytic abilities of thin films

The photocatalytic abilities of NTO and TiO₂ thin films were demonstrated by degrading surface-coated Rh B (Fig. S5 in ESI[†]). Rh B is a carcinogenic compound and it is often chosen as a model molecule for photocatalytic degradation. Both NTO and TiO₂ thin films show good photocatalytic ability under simulated AM 1.5 solar light irradiation (100 mW cm⁻²) at constant temperature of 25 °C (Fig. 5a). However, the photocatalytic abilities are different between NTO and TiO₂ thin films (Figs. 5a and b). The trend of the photocatalytic abilities is NTO-004 > NTO-RO > TiO₂-004 > TiO₂-RO. NTO-004

thin films show better photocatalytic performance than others because of the better light absorption and lower radiative recombination. After 2 hour irradiation, about 70% Rh B is degraded by NTO-004 thin films.

The photocatalytic activities depend on the surface morphology of thin films. The trend of calculated surface areas is TiO₂-004 > NTO-004 > TiO₂-RO = NTO-RO. Obviously, thin films with high degree of (004) orientation have larger contact area than those with random orientation. Therefore, both TiO₂ and NTO thin films with high degree of (004) orientation show better photocatalytic performance than those with random orientation. However, the thin film TiO₂-004 shows a poorer photocatalytic performance than NTO-RO, although it has a larger specific area than NTO-RO. This result is attributed to that NTO-RO could absorb the whole range spectrum of visible light, while TiO₂-004 is unable.

Fig. 5b shows reaction rates (k-value) of photocatalytic degradation for NTO and TiO₂ thin films. Only the NTO-004 thin film is found with a constant reaction rate, because Rh B could be completely and quickly degraded by NTO-004 thin films. The gradually decreasing reaction rates of other thin films are caused by the incomplete degradation of Rh B or poor photocatalytic ability. The complete and incomplete degradation of Rh B could be identified by the variation of the absorption spectra.³⁹ The absorption peaks of Rh B gradually decrease, suggesting cleavage of the whole chromophore structure of Rh B, namely complete degradation, eg. thin films with high degree of 004 orientation (Figs. S5b and d in ESI[†]). If only the N-deethylation occurs, then the Rh B is incomplete degradation and the absorption maximum will gradually shift

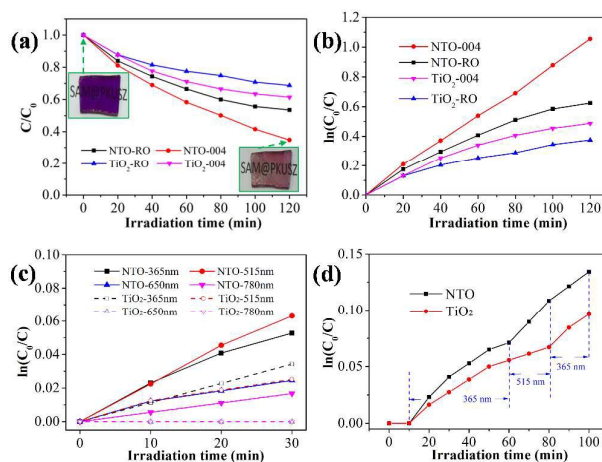


Fig. 5 (a) Comparison of the photocatalytic degradation rates of Rh B for NTO and TiO₂ thin films. The optical pictures show the initial and final state under simulated solar light irradiation. (b) The reaction rates (k-value) of photocatalytic degradation for NTO and TiO₂ thin films. (c) The reaction rates of photocatalytic degradation for NTO and TiO₂ thin films under different wavelengths irradiations. Lines of results for NTO-650 nm and TiO₂-515 nm are almost coincident. Lines of results for TiO₂-650 nm and TiO₂-780 nm are coincident. (d) The reaction rates of photocatalytic degradation for NTO and TiO₂ thin films under 365 and 515 nm irradiations. The films are without light irradiation for the initial 10 min.

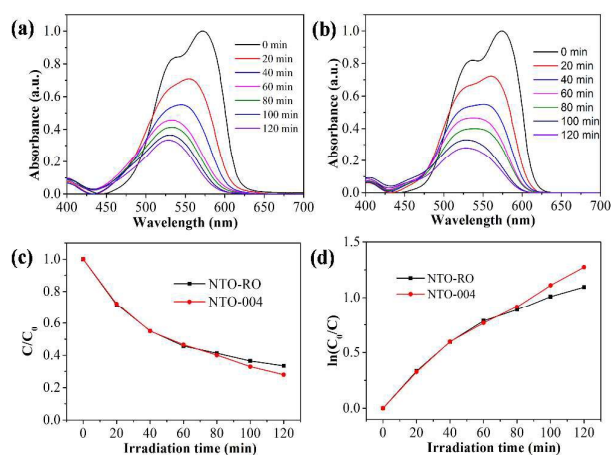


Fig. 6 Variation of the absorption spectra of a surface-coated Rh B degraded by NTO-RO (a) and NTO-004 (b) under simulated solar light irradiation. (c) Comparison of the photocatalytic degradation rates of Rh B for NTO-RO and NTO-004 thin films. (d) The reaction rates (k -value) of photocatalytic degradation for NTO-RO and NTO-004 thin films. The incident light is from the Rh B coating surface in these tests.

blue, eg. thin films with random orientation (Figs. S5a and c in ESI[†]). Therefore, the complete degradation of Rh B is of importance for photocatalytic reactions.

The photocatalytic abilities of NTO-004 and TiO₂-004 thin films were also demonstrated by degrading Rh B under single-wavelength LED irradiation. To avoid the intrinsic absorption of thin films, 365 (45.6 mW/cm²), 515 (45.8 mW/cm²), 650 (100 mW/cm²) and 780 nm (100 mW/cm²) LED irradiations were used (Fig. S6 in ESI[†]). NTO-004 thin films are active for photocatalysis under these wavelengths irradiations, indicating corresponding FCA is implemented in NTO-004 thin films. There is no free electron in the TiO₂ thin film, as a result it is only active under 365 and 515 nm irradiations (Fig. 5c). This result is in good agreement with our absorbance spectra analysis.

Amazingly, NTO-004 thin films show better performance under 515 nm of LED irradiation than that under 365 nm, while TiO₂-004 thin films show the opposite performance (Fig. 5c). This result is attributed to that the 515 nm irradiation light could be absorbed by both thin films and Rh B (Fig. S7 in ESI[†]). After being excited, Rh B can inject electrons into the conduction bands of both TiO₂-004 and NTO-004.^{40,41} However, only electrons injected into NTO-004 can be quickly transported and reused, because NTO-004 thin films have good conductive property.⁴² Electrons injected into TiO₂-004 are of noneffective utilization. This result indicates that Rh B could be photodegraded by NTO-004 thin films, even though incident light is blocked by the surface-coated dyes. This conclusion has been confirmed by an additional experiment as shown in Fig. 6. Both NTO-RO and NTO-004 show good photocatalytic activities, when the incident light is from the Rh B coating surface.

It should be noticed that reaction rates of NTO-004 gradually decrease under both 365 and 515 nm LED light sources irradiation (Fig. 5c). This result seems to be conflict with that under solar light irradiation (Fig. 5b). To make this

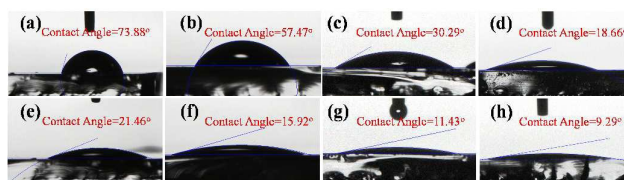


Fig. 7 Contact angles and optical pictures of as-prepared (a)-(d) and UV-treated (e-h) NTO and TiO₂ thin films. From left to right: TiO₂-RO, TiO₂-004, NTO-RO and NTO-004 thin films

clear, 365 and 515 nm LED light sources irradiation are used interchangeably for photocatalytic degradation. Reaction rates of both NTO and TiO₂ are gradually decreased under 365 nm irradiation (Fig. 5d). However, after 515 nm irradiation, reaction rates of all thin films are increased under latter 365 nm irradiation. This result indicates there might be a synergistic effect for photocatalytic performance when thin films were alternately irradiated under 365 nm and 515 nm LED.

3.5 The self-cleaning performance

A self-cleaning coating could remove pollutants and stains on its surface and save a lot of time and cost for maintenance of buildings, cars, outdoor facilities and solar panels.⁴³⁻⁴⁸ When applied as self-cleaning coatings, thin films should be hydrophobic or hydrophilic. TiO₂ and NTO thin films are of photo-induced hydrophilicity.⁴⁶⁻⁴⁸ However, some adsorbates are unable to be removed completely on both hydrophobic and hydrophilic surface, if rainwater is not abundant or energetic. Photocatalysts can transform the residual into harmless small molecules and remove it in a simple way via being exposed to sunlight. The combination of photocatalytic and hydrophilic properties makes the self-cleaning coating effective on both rainy and sunny days.

The wettability of both TiO₂ and NTO thin films was investigated by the contact angles. The contact angles are 73.88°, 57.47°, 30.29° and 18.66° for TiO₂-RO, TiO₂-004, NTO-RO and NTO-004 thin films, respectively (Figs. 7a-d). After UV irradiation, the contact angles can be decreased to 21.46°, 15.92°, 11.43° and 9.29°, respectively (Figs. 7e-h). All thin films show good hydrophilic properties and are suitable for self-cleaning coatings. The wettability is commonly related to the surface nanostructure of thin films. Compared with pure TiO₂ thin films, the particles are more sharply cone-shaped on the surface of NTO thin films (Fig. 3). Therefore, NTO thin films show better wettability than TiO₂ thin films. Moreover, cone-shaped particles distribute more densely on the surface of NTO-004 than that on the surface of NTO-RO, so NTO-004 shows better hydrophilic properties than others. These results indicate NTO thin films could perform as an effective self-cleaning coating for the glass.

Conclusions

In summary, we demonstrate a novel way to utilize the whole visible light to improve photocatalytic performance. After Nb doping, energy levels of TiO₂ are degenerate and corresponding carrier concentrations of thin films are on the

ARTICLE

Journal Name

order of 10^{21} cm^{-3} . These two aspects make NTO thin films absorb the whole range spectrum of visible light. The whole visible absorption is demonstrated by theoretical calculation, absorbance spectra and electrical properties. In addition, photocatalytic activities of thin films are also correlated with crystal orientation, surface morphology and photoluminescence spectra. NTO thin films with high degree of (004) orientation shows better photocatalytic performance than others due to the better absorption, the more effective charge transfer and the greater ability to completely degrade pollutants. In addition, a synergistic effect for photocatalytic performance is observed when thin films alternate irradiation between under 365 nm and 515 nm LED light. Finally, the combination of photocatalytic and hydrophilic properties makes NTO thin films suitable for self-cleaning coatings on both rainy and sunny days.

ORCID

Xiaoyang Yang: 0000-0001-6800-4110

Feng Pan: 0000-0002-8216-1339

Conflicts of interest

There are no conflicts to declare.

Acknowledgements

This work was supported by the financial support from the Shenzhen key science and technology plan (Grant No. JSGG20141118144410953), the Guangdong applied technology research special project (Grant No. 2015B090927003), and Shenzhen Science and Technology Innovation Committee Grant (Grant No. JCYJ20150331101121646).

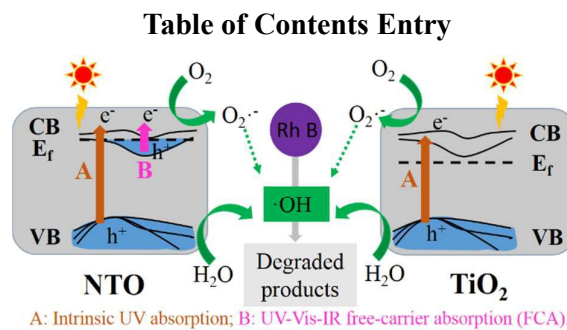
Notes and references

- J. Low, B. Cheng and J. Yu, *Appl. Surf. Sci.*, 2017, **392**, 658–686.
- M. M. Khin, A. S. Nair, V. J. Babu, R. Murugan and S. Ramakrishna, *Energy Environ. Sci.*, 2012, **5**, 8075–8019.
- M. Pelaez, N. T. Nolan, S. C. Pillai, M. K. Seery, P. Falaras, A. G. Kontos, P. S. M. Dunlop, J. W. J. Hamilton, J. A. Byrne, K. O'Shea, M. H. Entezari and D. D. Dionysiou, *Appl. Catal. B*, 2012, **125**, 331–349.
- J. Schneider, M. Matsuoka, M. Takeuchi, J. Zhang, Y. Horiuchi, M. Anpo and D. W. Bahnemann, *Chem. Rev.*, 2014, **114**, 9919–9986.
- J. Liu, Y. Liu, N. Liu, Y. Han, X. Zhang, H. Huang, Y. Lifshitz, S. T. Lee, J. Zhong and Z. Kang, *Science*, 2015, **347**, 970–974.
- C. Clavero, *Nat. Photonics*, 2014, **8**, 95–103.
- C. Wang, C. Shao, Y. Liu and X. Li, *Inorg. Chem.*, 2009, **48**, 1105–1113.
- A. Fujishima and K. Honda, *Nature*, 1972, **238**, 37–38.
- R. Asahi, T. Morikawa, H. Irie and T. Ohwaki, *Chem. Rev.*, 2014, **114**, 9824–9852.
- H. Choi, D. Shin, B. C. Yeo, T. Song, S. S. Han, N. Park and S. Kim, *ACS Catal.*, 2016, **6**, 2745–2753.
- N. Feng, Q. Wang, A. Zheng, Z. Zhang, J. Fan, S. B. Liu, J. P. Amoureux and F. Deng, *J. Am. Chem. Soc.*, 2013, **135**, 1607–1616.
- X. Yang, C. Cao, L. Erickson, K. Hohn, R. Maghirang and K. Klabunde, *Appl. Catal. B*, 2009, **91**, 657–662.
- R. Asahi, T. Morikawa, T. Ohwaki, K. Aoki and Y. Taga, *Science*, 2001, **293**, 269–271.
- X. Yue, S. Yi, R. Wang, Z. Zhang and S. Qiu, *J. Mater. Chem. A*, 2017, **5**, 10591–10598.
- J. Yu, J. Low, W. Xiao, P. Zhou and M. Jaroniec, *J. Am. Chem. Soc.*, 2014, **136**, 8839–8842.
- F. Mushtaq, A. Asani, M. Hoop, X. Z. Chen, D. Ahmed, B. J. Nelson and S. Pané, *Adv. Funct. Mater.*, 2016, **26**, 6995–7002.
- S. Khan, H. Cho, D. Kim, S. S. Han, K. H. Lee, S. H. Cho, T. Song and H. Choi, *Appl. Catal. B*, 2017, **206**, 520–530.
- L. Kong, C. Wang, F. Wan, L. Li, X. Zhang and Y. Liu, *Dalton Trans.*, 2017, **46**, 15363–15372.
- H. Y. Wang, J. Chen, F. X. Xiao, J. Zheng and B. Liu, *J. Mater. Chem. A*, 2016, **4**, 6926–6932.
- L. Kong, C. Wang, H. Zheng, X. Zhang and Y. Liu, *J. Phys. Chem. C*, 2015, **119**, 16623–16632.
- D. S. Bhachu, S. Sathasivam, G. Sankar, D. O. Scanlon, G. Cibin, C. J. Carmalt, I. P. Parkin, G. W. Watson, S. M. Bawaked, A. Y. Obaid, S. Al-Thabaiti and S. N. Basahel, *Adv. Funct. Mater.*, 2014, **24**, 5075–5085.
- B. N. Joshi, H. Yoon, M. F. A. M. V. Hest and Sam S. Yoon, *J. Am. Ceram. Soc.*, 2013, **96**, 2623–2627.
- J. Yang, X. Zhang, C. Wang, P. Sun, L. Wang, B. Xia and Y. Liu, *Solid State Sci.*, 2012, **14**, 139–144.
- K. A. Michalow, D. Flak, A. Heel, M. Parlinska-Wojtan, M. Rekas and T. Graule, *Environ. Sci. Pollut. Res.*, 2012, **19**, 3696–3708.
- A. Mattsson, M. Leideborg, K. Larsson, G. Westin and L. Osterlund, *J. Phys. Chem. B*, 2006, **110**, 1210–1220.
- X. Yang, M. J. Zhang, Y. Min, M. Xu, Z. Mei, J. Liang, J. Hu, S. Yuan, S. Xiao, Y. Duan, F. Liu, H. Lin, Y. Lin and F. Pan, *ACS Appl. Mater. Interfaces*, 2017, **9**, 29021–29029.
- H. G. Yang, C. H. Sun, S. Z. Qiao, J. Zou, G. Liu, S. C. Smith, H. M. Cheng and G. Q. Lu, *Nature*, 2008, **453**, 638.
- B. I. Stefanov, G. A. Niklasson, C. G. Granqvist and L. Osterlund, *J. Mater. Chem. A*, 2015, **3**, 17369–17375.
- F. Wang, G. Zhang, Z. Zhao, H. Tan, W. Yu, X. Zhang and Z. Sun, *Rsc Adv.*, 2015, **5**, 9861–9864.
- R. S. Zhang, Y. Liu, Q. Gao, F. Teng, C. L. Song, W. Wang and G. R. Han, *J. Alloys Compd.*, 2011, **509**, 9178–9182.
- A. Schleife, C. Rödl, F. Fuchs, K. Hannewald and F. Bechstedt, *Phys. Rev. Lett.*, 2011, **107**, 236405.
- E. Kioupakis, P. Rinke, A. Schleife, F. Bechstedt and C. G. Van De Walle, *Phys. Rev. B: Condens. Matter Mater. Phys.*, 2010, **81**, 2–5.
- H. Y. Fan, *Semicond. Semimetals*, 1967, **3**, 405–419.
- H. Peelaers, E. Kioupakis and C. G. Van De Walle, *Appl. Phys. Lett.*, 2012, **100**, 2010–2013.
- Y. Liu, J. M. Szeifert, J. M. Feckl, J. Rathousky, O. Hayden, D. Fattakhova-Rohlfing and T. Bein, *ACS Nano*, 2010, **4**, 5373–5381.
- G. E. Jellison, L. A. Boatner, J. D. Budai, B. S. Jeong, and D. P. Norton, *J. Appl. Phys.*, 2003, **93**, 9537–9541.
- Y. Furubayashi, T. Hitosugi, Y. Yamamoto, K. Inaba, G. Kinoda, Y. Hirose, T. Shimada and T. Hasegawa, *Appl. Phys. Lett.*, 2005, **86**, 252101.
- Y. Hirose, N. Yamada, S. Nakao, T. Hitosugi, T. Shimada and T. Hasegawa, *Phys. Rev. B*, 2009, **79**, 165108.

Journal Name

ARTICLE

- 39 J. Zhuang, W. Dai, Q. Tian, Z. Li, L. Xie, J. Wang, P. Liu, X. Shi and D. Wang, *Langmuir*, 2010, **26**, 9686–9694.
- 40 Y. K. Lee, J. Park and J. Y. Park, *J. Phys. Chem. C*, 2012, **116**, 18591–18596.
- 41 B. Gholamkhash, K. Koike, N. Negishi, H. Hori, T. Sano and K. Takeuchi, *Inorg. Chem.*, 2003, **42**, 2919–2932.
- 42 C. Chen, W. Ma and J. Zhao, *Chem. Soc. Rev.*, 2010, **39**, 4206–4219.
- 43 J. Y. Huang, S. H. Li, M. Z. Ge, L. N. Wang, T. L. Xing, G. Q. Chen, X. F. Liu, S. S. Al-Deyab, K. Q. Zhang, T. Chen and Y. K. Lai, *J. Mater. Chem. A*, 2015, **3**, 2825–2832.
- 44 K. Chen, S. Zhou and L. Wu, *Chem. Commun.*, 2014, **50**, 11891–11894.
- 45 R. Blossey, *Nat. Mater.*, 2003, **2**, 301–306.
- 46 M. J. Powell, R. Quesada-Cabrera, A. Taylor, D. Teixeira, I. Papakonstantinou, R. G. Palgrave, G. Sankar and I. P. Parkin, *Chem. Mater.*, 2016, **28**, 1369–1376.
- 47 Z. Zhao, H. Tan, H. Zhao, D. Li, M. Zheng, P. Du, G. Zhang, D. Qu, Z. Sun and H. Fan, *Chem. Commun.*, 2013, **49**, 8958–8960.
- 48 R. Rahal, T. Pigot, D. Foix and S. Lacombe, *Appl. Catal. B*, 2011, **104**, 361–372.



Niobium-doping makes both the intrinsic UV absorption and UV-Vis-IR free-carrier absorption occur in TiO_2 and improve photocatalytic performance.